RSC Advances

ROYAL SOCIETY OF CHEMISTRY

www.rsc.org/advances

Graphene oxide-based Fe_3O_4 nanoparticles as a novel scaffold for the immobilization of porcine pancreatic lipase

Yongbo Shao [a], Tao Jing*[a], Jingzhi Tian [a], Yongjie Zheng [a]

[a] *College of Chemistry and Chemical Engineering, Qiqihar University, Qiqihar 161006, China*

Professor, Tao Jing; jtkr@163.com; College of Chemistry and Chemical Engineering, Qiqihar University, Qiqihar 161006, China

Currently nano and hybrid materials has become a new approach for improving enzyme activity, stability and suitable for commercial application. In this paper, graphene oxide-based magnetic hybrids were prepared successfully. The chloropropyl-functioned graphene oxide decorated with Fe_3O_4 nanoparticles were made, noted as CPS/GO-Fe_3O_4@MCM-41. They were characterized by X-ray powder diffraction, scanning electron microscope, transmission electron microscope, fourier transform infrared spectroscopy, vibrating sample magnetometer, thermogravimetry and N_2 adsorption/desorption. Then the porcine pancreas lipase (PPL) was immobilized onto the graphene oxide-based magnetic nanoparticles via covalent bonding. The results showed that the novel supporting material CPS/GO-Fe_3O_4@MCM-41 was the best for PPL immobilization compared to the other two nanomaterials (GO-Fe_3O_4@MCM-41 and GO-Fe_3O_4). The supporting material CPS/GO-Fe_3O_4@MCM-41 exhibited enhanced immobilization efficiency (up to 98 %), maximum relative activity (up to 97.9 %), high stability and reusability (85 % 56 d and 87 % 10 cycles both at 30 °C). Additionally, it offered some other advantages, such as easy recycling and reusing, complying with the trend of green chemistry. Therefore, it is proposed that CPS/GO-Fe_3O_4@MCM-41 provide a new approach for commercial application.

Keywords: Graphene oxide, Fe_3O_4 nanoparticles, immobilization

Introduction

Graphene, a two-dimensional (2D) honeycomb lattice, is regarded as the 'thinnest material in the universe'. It offers outstanding thermal conductivity, mechanical strength, chemical stability, biocompatibility and non-toxicity, therefore, it has great future on the industrial applications [1-5]. Graphene oxide, a precursor of graphene, owns large surface area and plenty of functional groups, and exhibits good biocompatibility. Therefore, it is a good candidate for grafting other nanoparticles, and further immobilizing a large amount of enzymes. However, the difficulty is to separate the graphene oxide from the aqueous solution due to its strong hydrophility. The another hard thing is that nanosheet of graphene oxide inclines to agglomerate because of the strong π-π interactions between the nanosheets, which leads to the loss of surface area, so that many functional groups could be covered [6].

Fe_3O_4 nanoparticles can offer convenience of recovery due to the response to magnetic force, they have been adopted in catalytic, biological and drug delivery fields [7-12]. If integrated the graphene oxide with Fe_3O_4 nanoparticles, the combined supporting material can be separated rapidly with the addition of the external magnetic field. Meanwhile, the Fe_3O_4 nanoparticles can prevent the agglomeration of graphene oxide, so that the large surface area and the functional groups can be remained.

On the other hand, enzyme-catalyzed reactions have been applied extensively in industry due to their high efficiency, mild reaction conditions, non-toxicity, less by-products and environment friendly properties [13].

Among all the enzymes commercialized, porcine pancreatic lipase (PPL) is the one more common, cheaper and easier used, as it offers many advantages, including the high thermostability and water solubility. PPL is a small globular protein, which consisted of a single chain of 449 amino acids, and has a three-dimensional structure (molecular volume) of 4.6 nm × 2.6 nm × 1.1 nm. Its unique crystal structure looks like a lid that covers the catalytic site, which contains a catalytic triad: Ser, Asp and His at positions 153, 177 and 264, respectively [14].

As usual, the water-soluble enzyme shows some drawbacks, such as instability, easy deactivation and additional efforts to separate the enzymes from the product mixture. Therefore, the immobilized enzyme technology has been adopted and developed [15-17].

To date, PPL has been immobilized on various supports, and applied to various purposes. Unfortunately, some supports have low surface area and barely few functional groups or binding sites, which is inappropriate for the industrial applications. Therefore, it is still necessary to design a better efficient support for immobilizing enzymes.

In this regard, we designed a new supporting material, which was to integrate the graphene oxide with Fe_3O_4 nanoparticles, for the better immobilization of the enzyme. Meanwhile, we explored the relative activity, reusability and storage stability after the enzyme was immobilized to the new supporting material.

Experiment

1 Materials and methods

1.1 Materials

$FeCl_3 \cdot 6H_2O$, cetyltrimethylammonium bromide (CTAB), acetone, ethylene glycol, sodium acetate, absolute ethanol, absolute toluene, potassium permanganate, sodium nitrate, hydrogen peroxide, concentrated sulfuric acid and porcine pancreas lipase (PPL) powder (EC 3.1.1.3), 3000 (U/mL), (BR), were purchased from Sinopharm Chemical Reagent (Shanghai, China). Tetraethylorthosilicate (TEOS), ammonia (25 wt %), 3-chloropropyltriethoxysilane (CPS) and olive oil were purchased from Aladdin (Shanghai, China). Natural flake graphite was purchased from Qingdao Golden days of graphite company (Qingdao, China). All chemicals were of analytical-grade and without further purification.

1.2 Methods

1.2.1 Preparation of Fe_3O_4 nanoparticles

The preparation of Fe_3O_4 and Fe_3O_4@MCM-41 were according to the work as described previously [22].

1.2.2 Preparation of GO

Graphene oxide (GO) was prepared using the Hummers method [23]. Natural flake graphite (0.5 g) and sodium nitrate (2.5 g) were added into a round-bottom flask, which was set in ice-water bath, the concentrated sulfuric acid (115 mL, 36 N) was added and stirred slowly. Afterwards, potassium permanganate (15 g) was added and mixed. The mixture was kept in the ice-water bath for 2 h, then transferred the flask into a thermostat water bath, and stirred for 30 min at 35 °C. After that, the flask was transferred into the ice-water bath again, and added deionized water (230 mL) gradually. The temperature would be increased. Transferred the flask into thermostat water bath again, and stirred for 20 min at 98 °C. The reaction mixture was then cooled down naturally to room temperature. Subsquently, the hydrogen peroxide (250 mL) was added. By now, a bright yellow solution was obtained, collected the precipitate by centrifugation and washed it with diluted hydrochloric acid, the supernatant was collected and detected with barium chloride solution. Then the precipitate was washed with distilled water until the pH of supernatant reached to neutral.

1.2.3 Preparation of CPS/GO-Fe_3O_4@MCM-41

Fe_3O_4@MCM-41 (0.3 g) was dispersed in absolute ethanol (60 mL) and sonicated for 30 min. Meanwhile, GO was also dispersed in distilled water (0.5 mg/mL). Mixed the two solutions (3: 4/v: v) prepared above and stirred vigorously for 1 h. Then 3-chloropropyltriethoxysilane (CPS) (1 mL) was dropped into the above solution generated above, stirred vigorously at 120 °C, refluxed for 10 h, washed with absolute ethanol for several times and freeze-dried. The product was noted as CPS/GO-Fe_3O_4@MCM-41. For comparison, GO-Fe_3O_4 and GO-Fe_3O_4@MCM-41 were also prepared by the same process except the addition of 3-chloropropyltriethoxysilane (Fig. 1).

1.2.4 Immobilization of PPL on CPS/GO-Fe_3O_4@MCM-41, GO-Fe_3O_4@MCM-41 and GO-Fe_3O_4

CPS/GO-Fe_3O_4@MCM-41 (0.36 g) was equilibrated in the PBS buffer (10.0 mL; pH 7.5, 0.05 M) at 25 °C for 1 h, which was named supporting solution. PPL (0.036 g)

was dissolved in the PBS buffer (10.0 mL; pH 7.5, 0.05 M) to obtain a solution, which was then added into the supporting solution mentioned above. The resulting mixture was shaken for 12 h at 150 r/min (25 °C). Afterwards, the immobilized PPL material was collected, washed with enough PBS buffer and stored at 4 °C until use. The other two immobilized PPL materials were obtained according to the same process mentioned above.

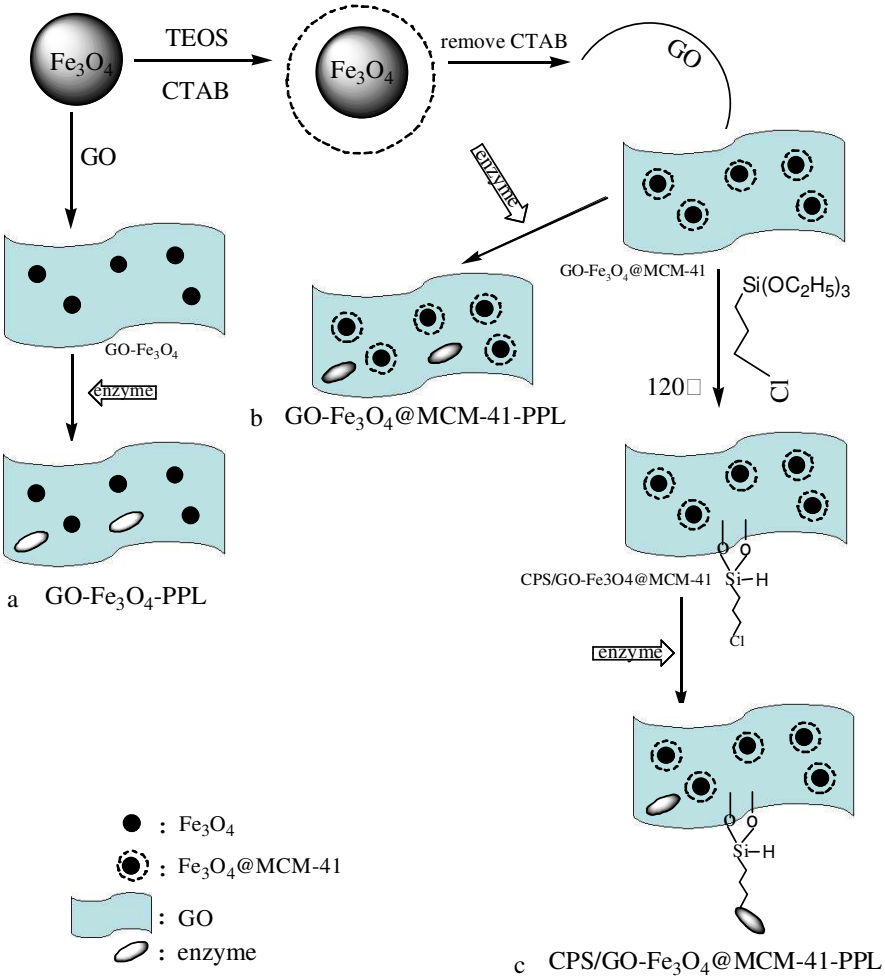

Fig. 1 Schematic representation for the formation of (a) GO-Fe_3O_4-PPL, (b) GO-Fe_3O_4@MCM-41-PPL and (c) CPS/GO-Fe_3O_4@MCM-41-PPL

1.2.5 Immobilization efficiency of PPL

Immobilization efficiency of PPL on nanoparticles was determined by the Bradford method as described previously [24]. Briefly, the absorbance of solution was measured at 595 nm using UV-visible spectroscopy first, and then the percentage of

the immobilized PPL was calculated by subtracting the PPL content in the supernatant from the total as follows.

Immobilization efficiency (%) = (total PPL content (mg/ml) - PPL content in the supernatant (mg/ml)) / total PPL content * 100%.

The optimal concentration of the enzyme was 0.35 mg/mL for CPS/GO-Fe_3O_4@MCM-41-PPL, 0.30 mg/mL for GO-Fe_3O_4@MCM-41-PPL, and 0.25 mg/mL for GO-Fe_3O_4-PPL, respectively.

1.2.6 Activity assay

The activity of PPL and immobilized-PPL were determined by use of olive oil as the substrate [22]. One unit (U) of the PPL activity was defined as the amount of lipase releasing 1 μmol of fatty acid per minute. The initial activity (3000 U/mL) of PPL was defined as the maximum activity (100 %).

1.2.7 The effect of temperature on PPL relative activity

The effect of temperature on relative activity was investigated as follows: the immobilized PPL and non-immobilized PPL (3.6 mg/mL for both) were added into the PBS buffer (pH 7.5, 0.05M) and kept for 1 hour at the temperature of 25 °C, 30 °C , 35 °C, 40 °C, 45 °C, 50 °C, 55 °C and 60 °C, respectively.

1.2.8 The effect of the pH on PPL relative activity

The effect of pH on PPL relative activity was investigated under the conditions of 30 °C for 1 h, and the PBS buffer pH values was adjusted to 5.5, 6.0, 6.5, 7.0, 7.5, 8.0, 8.5, and 9.0, respectively.

1.2.9 Reusability and storage stability of the immobilized PPL

The reusability was studied as follows. The relative activity of the immobilized PPLs (3.6 mg/mL) was measured after each run and up to ten runs with the conditions of 30 C, pH 7.5 and 1 hour reaction time. After each run, the immobilized PPL was recovered with the aid of magnet, washed with PBS buffer (pH 7.5, 0.05 M) for three times. The storage stability of the immobilized PPL and non-immobilized PPL were determined based on the days that the activity lasted for. The activity was tested every 7 days with the conditions of 30 °C at pH 7.5.

1.3 Characterizations

X-ray diffraction (XRD) spectra of the samples were studied using a Bruker, D8-FOCUS diffractometer equipped with Cu/Kα radiation at a scanning rate of 4°-8° min^{-1}. Fourier transform infrared spectroscopy (FTIR) (Spectrum One B, PE) was used for detecting the functional groups of materials in the range of 400-4000cm^{-1}. Magnetic susceptibility were measured using a vibrating sample magnetometer (VSM) (VersaLab VL-072, Quantum Design) in the magnetic field sweeps off -30,000 Oe to -30,000 Oe at room temperature. Morphological characteristics of the samples were measured with Hitachi S-4300 scanning electron microscope (SEM) and Hitachi S-7650 Transmission electron microscopy (TEM). For investigating the surface area and pore size, the samples were first degassed in a vacuum at 77K for 3h, and then tested with Surface Area & Pore Size Analyzer (AUTOSORB-1, Quantachrome). Thermogravimetric analysis (TGA) was conducted by use of the NETZSCH STA 449 F3 Jupilter thermo-analyzer in the temperature range 0-800 °C at a heating rate of 10 °C min^{-1}. The surface composition inspection and the valence states of the samples were measured by X-ray photoelectron spectroscopy (XPS) (ESCALAB250Xi, Thermo Company).

Results and discussion

2.1 Materials characterizations

2.1.1 Morphological characteristics observed by SEM and TEM images

The SEM and TEM images for Fe_3O_4, Fe_3O_4@MCM-41, GO, GO-Fe_3O_4, GO-Fe_3O_4@MCM-41 and CPS/GO-Fe_3O_4@MCM-41 were shown in Fig. 2. Before coating, the shape of Fe_3O_4 nanoparticles was spherical, the size was about 300 nm, and displayed good dispersancy (a, c). After coated by the mesoporous silicon (MCM-41), the shape of Fe_3O_4@MCM-41 was also spherical, but the size was increased to 500 nm, and showed the orderly and closely arrangement (b, d). Compared to the Fe_3O_4, the surface of the Fe_3O_4@MCM-41 became smoother (b). Morphologically, the Fe_3O_4 nanoparticles were coated by mesoporous silicon evenly [25]. The morphology of GO was shown in Fig. 2 (e), in which a four layered

structure was observed. It was thin, transparent, and accompanied with several micrometer-long wrinkles. As shown in Fig. 2 (f, g and h), Fe_3O_4 and Fe_3O_4@MCM-41 nanoparticles located on the surface of GO layers were tightly wrapped by the wrinkled and ultrathin GO sheet [26]. These results showed that the materials used in the experiments were prepared successfully.

a)

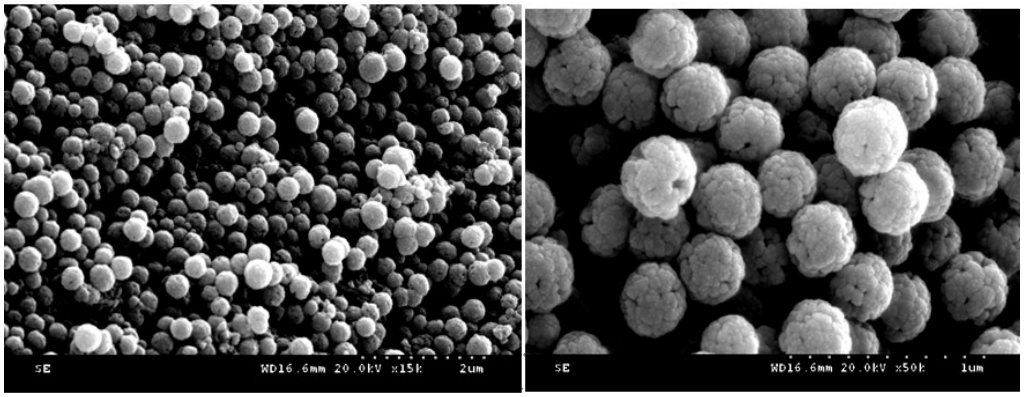

b)

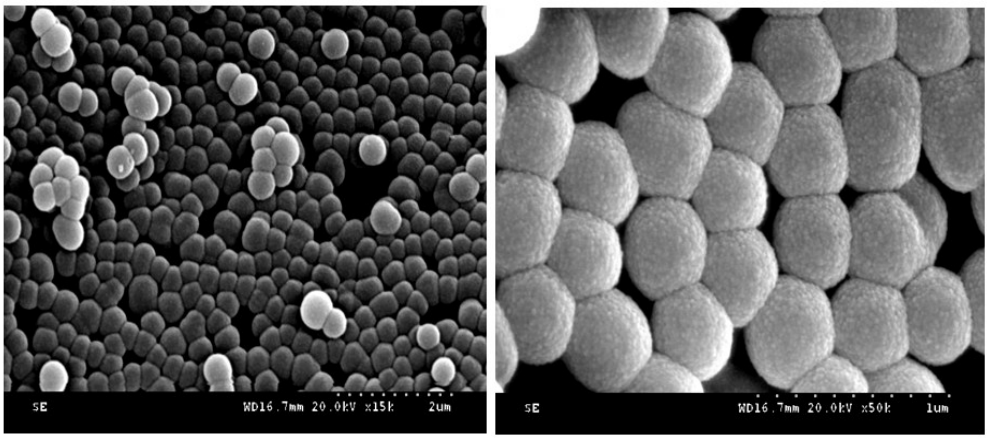

c) d)

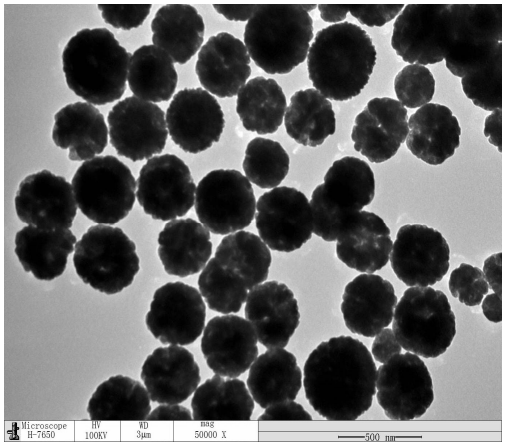

e)

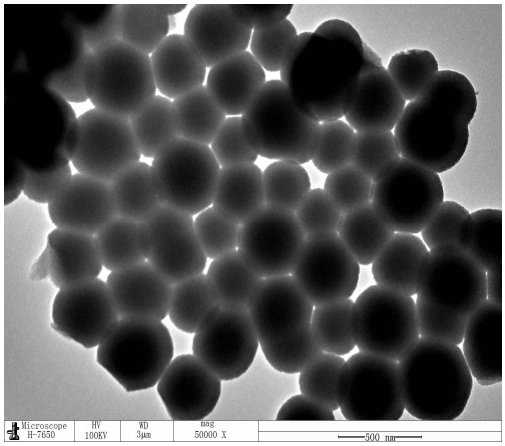

f)

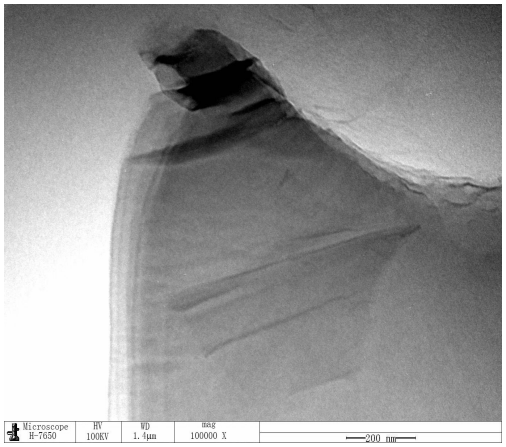

g)

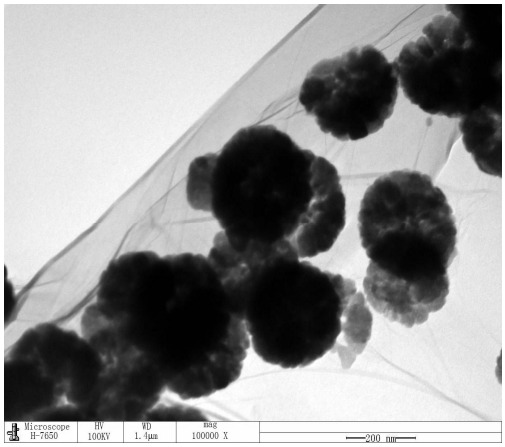

h)

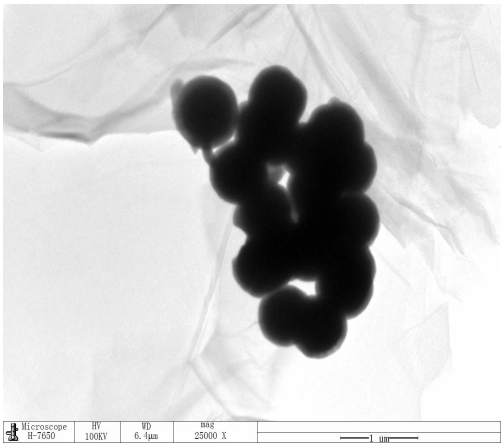

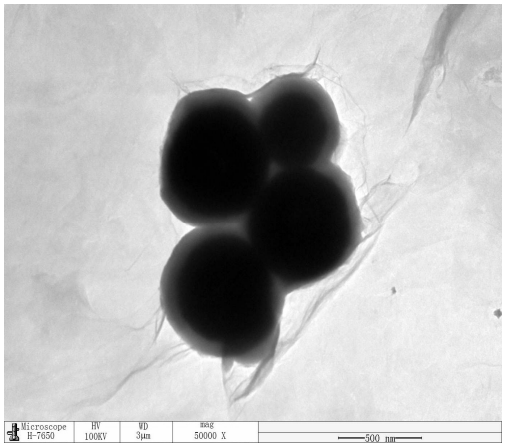

Fig. 2 SEM images of (a) Fe_3O_4; (b) Fe_3O_4@MCM-41 and TEM images of (c) Fe_3O_4; (d) Fe_3O_4@MCM-41; (e) GO; (f) GO-Fe_3O_4; (g) GO-Fe_3O_4@MCM-41 and (h) CPS/GO-Fe_3O_4@MCM-41

2.1.2 Determination of crystal structure by XRD analysis

The crystal structures of Fe_3O_4, Fe_3O_4@MCM-41, GO and CPS/GO-Fe_3O_4@MCM-41 were characterized by powder X-Ray diffraction (XRD) (Fig. 3). The structures of Fe_3O_4@MCM-41 and CPS/GO-Fe_3O_4@MCM-41 were characterized by small angle X-ray analysis in the range of 1°-6°. The result from the small angle X-ray analysis for CPS/GO-Fe_3O_4@MCM-41 was the same as the result for Fe_3O_4@MCM-41 (Fig. 3 (c)) exactly, the only characteristic peaks were observed at 2θ of 2.0°, which was attributed to the short-range ordering features of the mesopore alignment on the spherical surface [22]. The wide angle analysis of XRD revealed six characteristic peaks for Fe_3O_4, which were located at 2θ of 30.2°, 35.4°, 42.9°, 53.5°, 57.0° and 62.4°.These peaks were assigned to the crystal plane (220), (311), (400), (422), (511) and (440), respectively. For Fe_3O_4@MCM-41, the peak at 2θ of 18–24° represented the amorphous phase of SiO_2. The XRD pattern of GO was shown in Fig. 3 (d). The unique characteristic peak was observed at 2θ of 10.5°, which was assigned to the crystal plane (001). The XRD pattern of CPS/GO-Fe_3O_4@MCM-41 was shown in Fig. 3 (e), where the characteristic diffraction peak of GO was not observed, however, the six characteristic peaks of Fe_3O_4 were reserved [27]. These results indicated that Fe_3O_4, Fe_3O_4@MCM-41, GO and CPS/GO-Fe_3O_4@MCM-41 were prepared successfully.

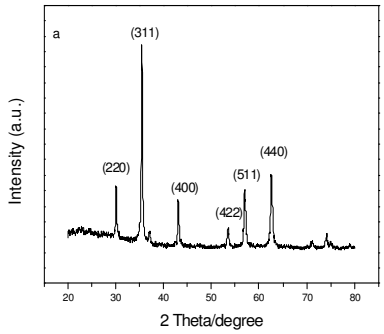

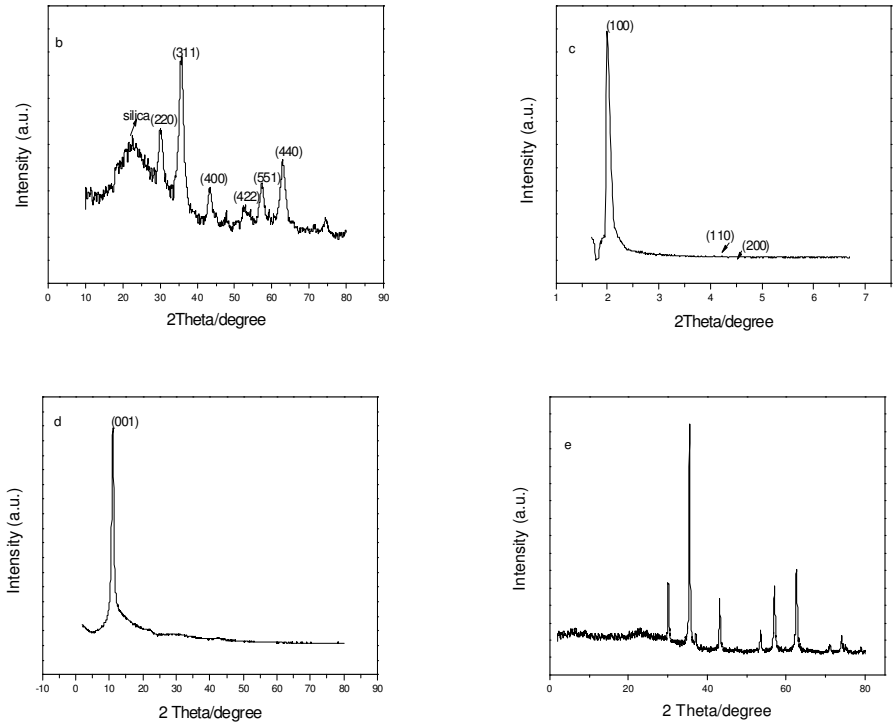

Fig. 3 XRD patterns of the (a) Fe_3O_4, (b) Fe_3O_4@MCM-41, (c) small angle X-ray analysis of Fe_3O_4@MCM-41 and CPS/GO-Fe_3O_4@MCM-41, (d) GO and (e) CPS/GO-Fe_3O_4@MCM-41

2.1.3 X-ray photoelectron spectroscopy (XPS) analysis

The surface composition and the valence states of the samples were investigated by the XPS spectroscopy spectra, as shown in Fig. 4. The wide scan XPS spectra of the samples was shown in Fig. 4 (a), and displayed the sharp peaks at the binding energy of 285, 530, 711, 101 and 199 eV, which were assigned to C 1s, O 1s, Fe 2p, Si 2p and Cl 2p, respectively. The result indicated the existence of C, O, Fe, Si and Cl in the corresponding samples. The high-resolution XPS spectra of Fe 2p scan was shown in Fig. 4 (b). The peaks at 711.2 eV and 725.6 eV could be assigned to Fe $2p_{3/2}$ and Fe $2p_{1/2}$, respectively. The peak around 720 eV of γ-Fe_2O_3 was not observed, suggesting that the only form of Fe_3O_4 existed in GO-Fe_3O_4, GO-Fe_3O_4@MCM-41 and CPS/GO-Fe_3O_4@MCM-41 [28]. The Si 2p spectra of GO-Fe_3O_4@MCM-41 were shown in Fig. 4 (c). The two peaks at 101.3 eV and 102.3 eV were assigned to the

Si-O-C and Si-O-Si, respectively, which suggested that there were two chemical states of Si. This result was consistent with the conclusion from the FTIR analysis (Fig. 5). The C1s spectra of GO, GO-Fe_3O_4, GO-Fe_3O_4@MCM-41 and CPS/GO-Fe_3O_4@MCM-41 were shown in Fig. 4 (d, e, f and g). The deconvoluted peaks of GO were displayed at four positions corresponding to C=C sp^2 (284.4 eV), C-C sp^3 (285.1 eV), C-OH and/or C-O-C (286.9 eV), C=O (288.9 eV) [28]. The peak of C-C sp^3 in GO-Fe_3O_4, GO-Fe_3O_4@MCM-41 and CPS/GO-Fe_3O_4@MCM-41 shifted to higher binding energy by 0.1 eV, 0.1 eV and 0.6 eV, respectively. In addition, the intensity of C=C sp^2 peak in GO-Fe_3O_4, GO-Fe_3O_4@MCM-41 or CPS/GO-Fe_3O_4@MCM-41 was increased compared to the one in GO. Together, it was believed that the magnetic mesoporous silicon grafted onto the surface of GO sheet [28]. The peaks of C-OH and/or C-O-C in GO-Fe_3O_4 and GO-Fe_3O_4@MCM-41 were greatly decreased compared to the one in GO. It was even decreased more while CPS was grafted onto the surface of GO sheet. These results suggested that GO was partly reduced in the modified nanomaterials [27, 28]. The N 1s spectra of PPL and CPS/GO-Fe_3O_4@MCM-41-PPL were shown in Fig. 4 (h and i). The sharp peak at the binding energy of 399.8 eV was assigned to N 1s for PPL. While the peak in CPS/GO-Fe_3O_4@MCM-41-PPL shifted to higher binding energy by 0.5 eV. The result indicated that the PPL was bound to the CPS/GO-Fe_3O_4@MCM-41 by covalent attachment [29, 30]. All the results from the x-ray photoelectron spectroscopy (XPS) analysis demonstrated that the supporting materials were prepared successfully.

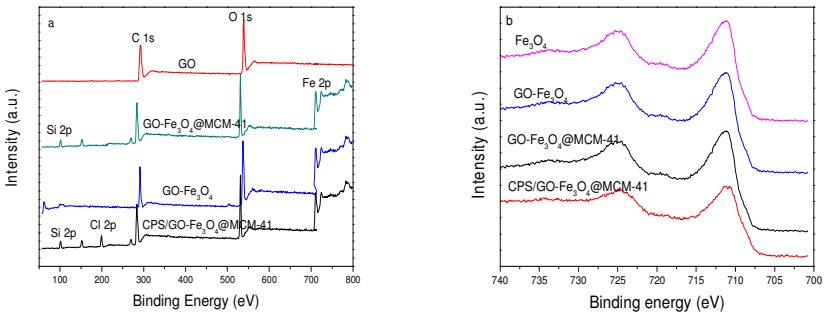

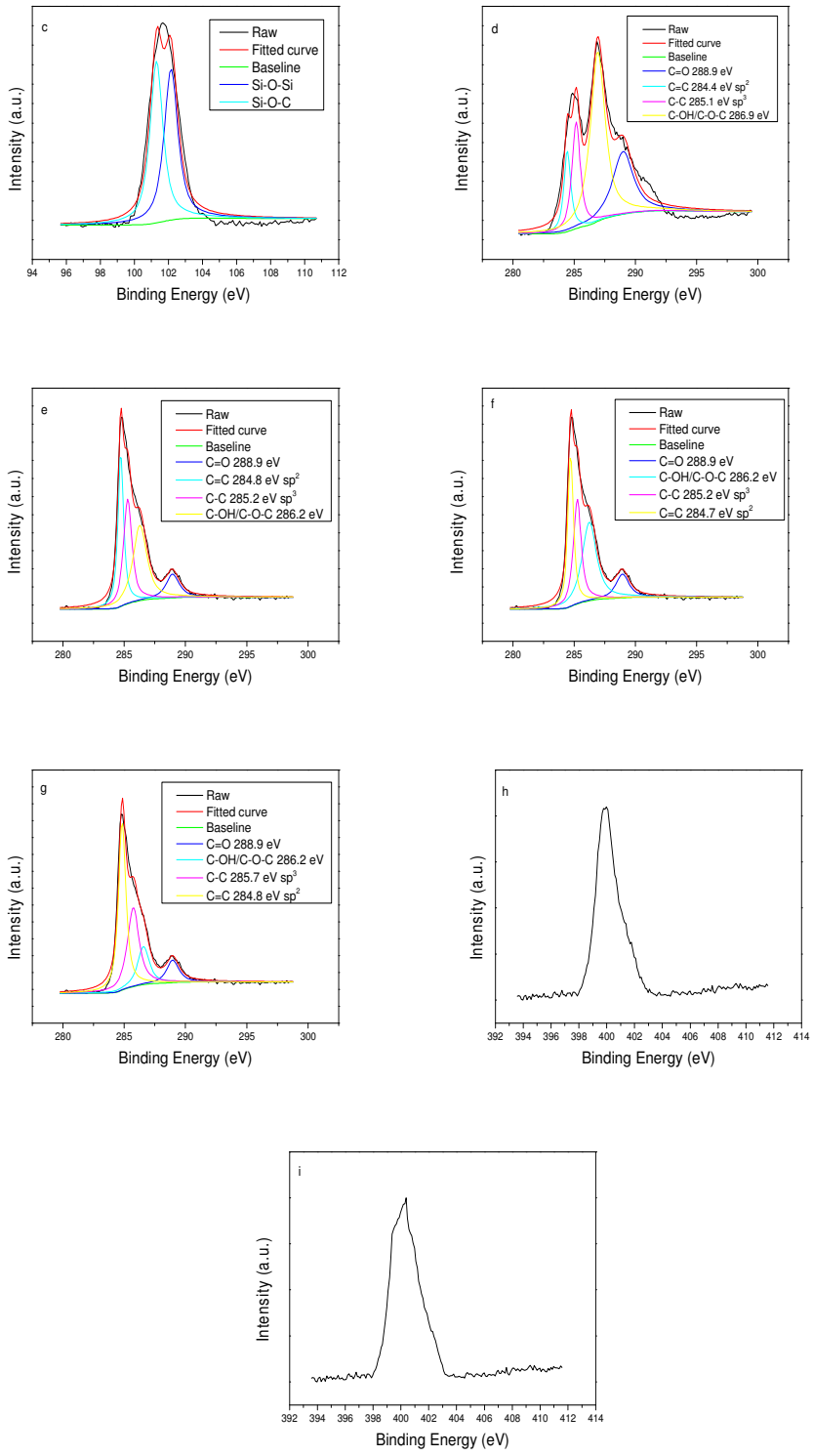

Fig. 4 XPS spectra scan (a) wide scan XPS spectra of the supporting materials, (b) high-resolution XPS spectra of Fe 2p scan, (c) Si 2p spectra of GO-Fe_3O_4@MCM-41, C 1s spectra of (d) GO, (e) GO-Fe_3O_4, (f) GO-Fe_3O_4@MCM-41, (g)

CPS/GO-Fe_3O_4@MCM-41 and N 1s spectra of (h) PPL and (i) CPS/GO-Fe_3O_4@MCM-41-PPL

2.1.4 The functional groups by FT-IR spectra analysis

FT-IR spectra of GO-Fe_3O_4@MCM-41 (a), GO-Fe_3O_4 (b), GO (c), CPS/GO-Fe_3O_4@MCM-41 (d) and Fe_3O_4 (e) were shown in Fig. 5. For the results of Fe_3O_4 (e), the peaks at 582 cm^{-1}, 1629 cm^{-1} and 3423 cm^{-1} indicated the vibration of the Fe-O bond, the bending vibration of the O-H bond and the stretching vibration of the O-H group, respectively. In the curve of GO (c), the peaks at 1733 cm^{-1}, 1621 cm^{-1}, 1226 cm^{-1} and 1061 cm^{-1} were assigned to C=O stretching vibration of carbonyl and carboxyl groups located at edges of the GO networks, C=C vibration of skeleton, C-OH vibration and C-O stretching vibration of epoxide group, respectively [31]. For the GO-Fe_3O_4 spectrum (b), the peak of C=O was observed with lower intensity compared to GO spectrum (c), suggesting that the GO sheet was partly reduced, which was consistent with the XPS results (Fig. 4). In addition, the wavelengh of Fe-O bond was shifted to lower wavelengh of 576 cm^{-1} compared to 582 cm^{-1} in Fe_3O_4 nanoparticles. It was suggested that Fe_3O_4 nanoparticles were grafted onto the GO sheet [32]. In the spectrum of GO-Fe_3O_4@MCM-41 (a) and CPS/GO-Fe_3O_4@MCM-41 (d), the peaks at 470 cm^{-1} and 801 cm^{-1} were attributed to the characteristic vibrations for the framework (Si-O-Si) of mesoporous. The vibration peaks at 1095 cm^{-1} and 1041 cm^{-1} were attributed to the Si-O-Si and Si-O-C groups, suggesting that the magnetic mesoporous silicon was grafting on the surface of GO by the covalent attachment [33]. After the modification with mesoporous silicon, the intensity of peaks at 2925 cm^{-1} and 2854 cm^{-1} were increased, which were attributed to the symmetric and asymmetric stretching of $-CH_3$ and $-CH_2$ groups, respectively. The peak of the O-H bond at 3423 cm^{-1} was decreased and assigned that the GO sheet was decorated with the magnetic mesoporous silicon [34]. In the curve of CPS/GO-Fe_3O_4@MCM-41, the vibration peak at 691 cm^{-1} was attributed to the C-Cl bond. The new bonds at 1645 cm^{-1} and 1573 cm^{-1} were assigned that 3-chloropropyltriethoxysilane (CPS) was bound to the $-COO^-$ on the GO sheet[33, 34].

For the immobilized PPL spectrum, the peak at 2939 cm^{-1}, specific for N-H bond, was observed in all the curves (GO-Fe_3O_4@MCM-41-PPL (f), GO-Fe_3O_4-PPL (g), PPL (h) and CPS/GO-Fe_3O_4@MCM-41-PPL (i)), which confirmed that PPL remained in the supporting materials. The O-H peak at 3390 cm^{-1} was decreased when the enzyme was adsorbed onto the GO-Fe_3O_4@MCM-41 and GO-Fe_3O_4. These results suggested that the N-H groups of PPL interacted with O-H groups of the supporting materials via hydrogen bonding [35]. In addition, the GO sheet was partly reduced in the process (Fig. 4), we proposed that PPL was immobilized onto the surface (GO-Fe_3O_4@MCM-41 and GO-Fe_3O_4) mainly in the form of hydrogen bonding with the hydroxyl groups. For the CPS/GO-Fe_3O_4@MCM-41-PPL spectrum (i), the peak for C-N bond was not observed because it was overlapped by strong Si-O-Si and Si-O-C bonds at 1200-900 cm^{-1} [36]. However, the C-Cl bond in the CPS/GO-Fe_3O_4@MCM-41-PPL disappeared, suggesting that the enzyme was immobilized on the supporting materials. All the results from the FT-IR spectra indicated that the supporting materials were prepared well, and the PPL was immobilized on them successfully.

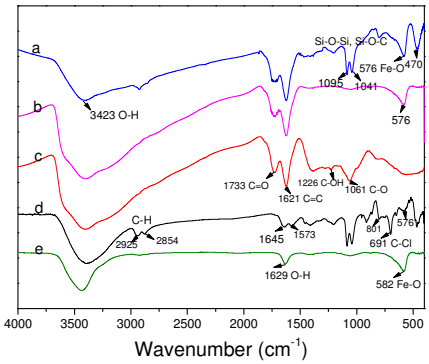

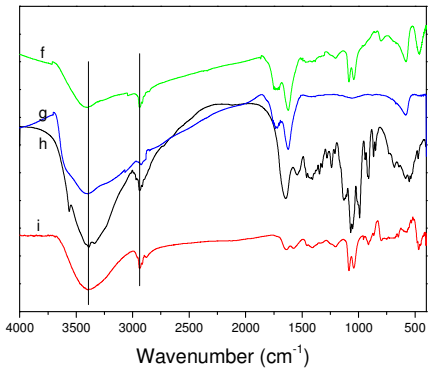

Fig. 5 FTIR spectra for the supporting materials and the immobilized PPL

2.1.5 Magnetic properties by VSM analysis

The magnetic properties of differently synthesized nanoparticles were measured using a vibrating sample magnetometer at room temperature (Fig. 6). The saturation magnetizations (*Ms*) for GO-Fe_3O_4, GO-Fe_3O_4@MCM-41 and CPS/GO-Fe_3O_4@MCM-41 were 81 emu/g, 66 emu/g, and 45 emu/g, respectively. The *Ms* of the samples were gradually weakened, suggesting that the Fe_3O_4 nanoparticles were coated by mesoporous silica, and further modified with CPS. These phenomena were consistent with the results from FTIR, SEM, TEM and XRD. Fig. 6 (b) showed the magnified magnetic field of the samples ranging from -3000 Oe to 3000 Oe, the remanence magnetization and coercivity were very small, suggesting that all the samples exhibited ferromagnetic behaviors. The contract figure of CPS/GO-Fe_3O_4@MCM-41 with the magnetic field was displayed in Fig. 6 (c). It showed that the introduction of the magnet made the separation of the supporting materials from the solution phase efficiently.

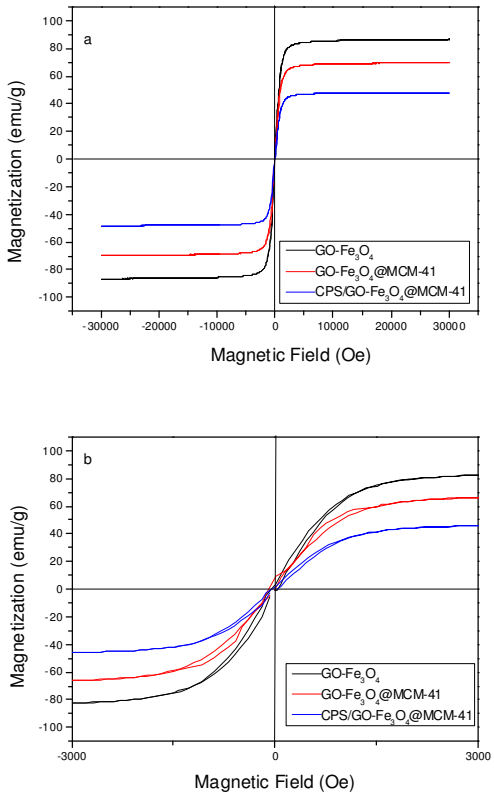

c)

Fig. 6 VSM curves for GO-Fe_3O_4, GO-Fe_3O_4@MCM-41 and CPS/GO-Fe_3O_4@MCM-41 (a) Magnetic field from -30000 Oe to 30000 Oe (b) Magnetic field from -3000 Oe to 3000 Oe (c) and the contract figures of CPS/GO-Fe_3O_4@MCM-41 with the magnetic field

2.1.7 Thermal behaviors by TGA analysis

The thermal behaviors of GO and CPS/GO-Fe_3O_4@MCM-41 were characterized by TGA in a nitrogen environment, as shown in Fig. 7. Based on the curve of GO, the

initial weight loss occurred at lower temperatures (below 100 °C) because the residual water was lost at the beginning. The second weight loss occurred at temperatures from 150 °C to 300 °C, it was attributed to the decomposition of the oxygen-containing groups of GO [36]. The third weight loss (from 300 °C to 650 °C) was assigned to the breakdown of the -COOH group in GO [38]. For the CPS/GO-Fe_3O_4@MCM-41 curve, the weight loss below 150 °C was assigned to the loss of residual water and absorbed solvent. The second weight loss occurred at the temperatures ranging from 150 °C to 417 °C, and it was attributed to the burning of the residual oxygen-functioned groups of CPS/GO-Fe_3O_4@MCM-41 [27]. The third weight loss at 417-700 °C was ascribed to the decomposition of the chloropropyl groups and carbon frame of the graphene [39]. From the results of TGA, the loading amount of CPS occupied 10 wt% among the CPS/GO-Fe_3O_4@MCM-41.

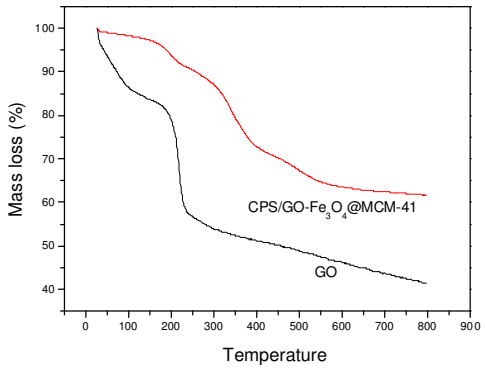

Fig. 7 TGA curves of GO and CPS/GO-Fe_3O_4@MCM-41

2.1.8 Pore structure and distribution by nitrogen adsorption/desorption isotherm analysis

Nitrogen adsorption/desorption isotherm analysis were performed on these materials to investigate their porous structure and surface area, as shown in Fig. 8. For the pure Fe_3O_4 (a), the isotherm exhibited type II according to IUPAC classification without hysteresis loop [40]. The isotherms for the other four nanomaterials were all close to the Type IV isotherm with a hysteresis loop in the 0.4-1.0 range of relative pressure, which were typical characteristics of mesoporous structure. The surface area was 484.10 m^2/g for GO (b), 234.32 m^2/g for GO-Fe_3O_4 (c), 200.09 m^2/g for

GO-Fe_3O_4@MCM-41 (d) and 191.58 m^2/g for CPS/GO-Fe_3O_4@MCM-41 (e). The results were attributed to the fact that Fe_3O_4 nanocomposites easily aggregated together [40]. In addition, the surface areas of the graphene oxide-based Fe_3O_4 nanoparticles increased compared to the pure Fe_3O_4 nanoparticles (89.51 m^2/g). The pore volume and pore size of GO, GO-Fe_3O_4, GO-Fe_3O_4@MCM-41 and CPS/GO-Fe_3O_4@MCM-41 gradually decreased when the Fe_3O_4 nanocomposites and 3-chloropropyltriethoxysilane (CPS) anchored on GO sheets (Table 1), which was consistent with the other study [40].

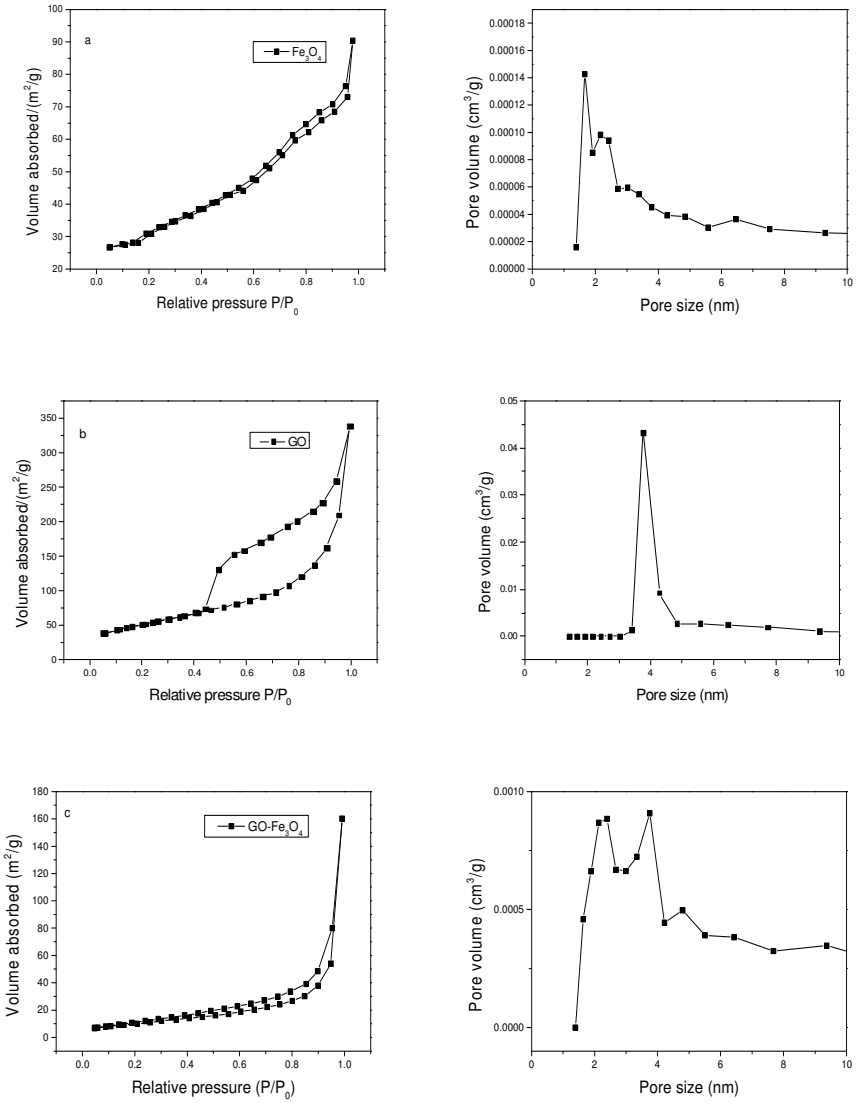

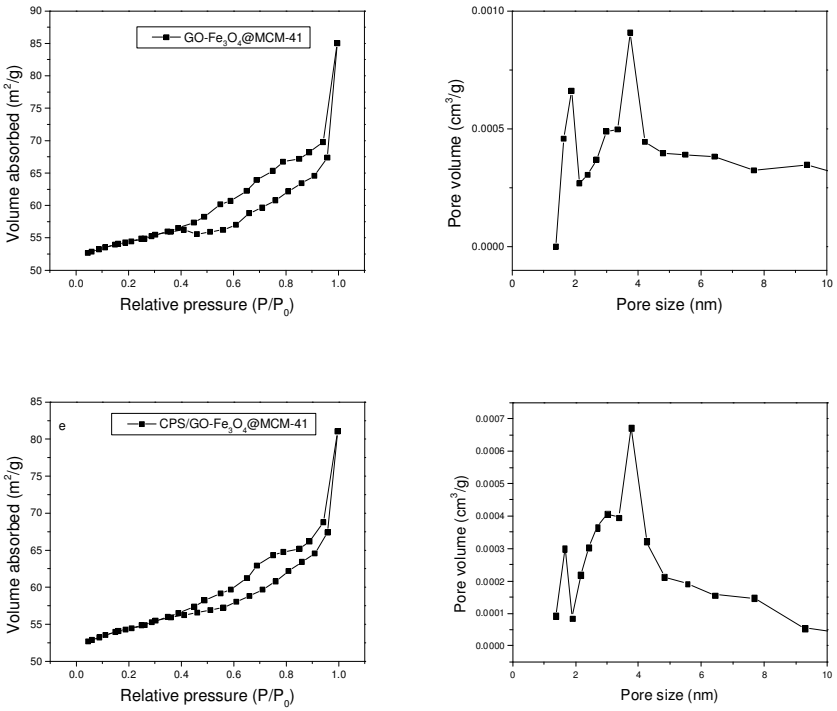

Fig. 8 Nitrogen adsorption/desorption isotherms and pore size distribution of (a) Fe_3O_4, (b) GO, (c) GO-Fe_3O_4, (d) GO-Fe_3O_4@MCM-41 and (e) CPS/GO-Fe_3O_4@MCM-41

Table 1 surface area, pore volume and pore size

samples	surface area (m^2/g)	pore volume (cm^3/g)	pore size (nm)
Fe_3O_4	89.51	0.11	1.85
GO	484.10	0.52	3.70
GO-Fe_3O_4	234.32	0.25	3.00
GO-Fe_3O_4@MCM-41	200.09	0.20	2.93
CPS/GO-Fe_3O_4@MCM-41	191.58	0.13	2.65

2.2 PPL immobilization

The amount of the PPL immobilized on CPS/GO-Fe_3O_4@MCM-41, GO-Fe_3O_4@MCM-41 and GO-Fe_3O_4 were investigated using an ultraviolet-visible spectrophotometer, as shown in Fig. 9. The results indicated that the amount of the

PPL immobilized on different supporting materials was varied. Under the optimal conditions, 98 % of PPL were immobilized onto the CPS/GO-Fe_3O_4@MCM-41, 88 % of PPL were immobilized onto the GO-Fe_3O_4@MCM-41, and 76 % of PPL were immobilized onto the GO-Fe_3O_4 (based on the equation mentioned in the Methods section). It was clear that CPS/GO-Fe_3O_4@MCM-41-PPL was better than the other two supporting materials. It was speculated that 3-chloropropyltriethoxysilane (CPS), as a spacer, could reduce steric hindrance, so that more enzymes could bind to the surface of the supporting materials [41]. Secondly, the covalent attachment also played an important role in the performance. Thirdly, magnetic mesoporous silicon was deposited on the surface of graphene oxide, which provided more surface area and more chemical functional groups that could absorb some PPL [42].

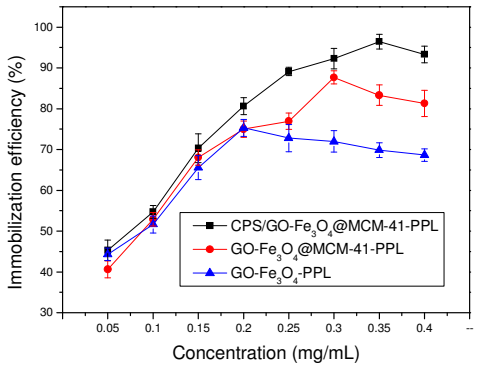

Fig. 9 Effect of the concentration of PPL on immobilization efficiency

2.3 Relative activity of the immobilized PPL

2.3.1 The effect of the immobilized PPL concentration on the relative activity

The relative activity varied with the concentration of the non-immobilized PPL and immobilized PPL (Fig. 10). The highest relative activity was obtained when the concentration of CPS/GO-Fe_3O_4@MCM-41-PPL, GO-Fe_3O_4@MCM-41-PPL, GO-Fe_3O_4-PPL and non-immobilized PPL were 0.35 mg/mL, 0.30 mg/mL, 0.30 mg/mL and 0.25 mg/mL, respectively. As shown in Fig. 9, it was clear that the relative activity of the CPS/GO-Fe_3O_4@MCM-41-PPL (97.9 % of initial activity) was the highest when the enzyme concentration was kept in optimum. Again, this could be mainly attributed that CPS/GO-Fe_3O_4@MCM-41-PPL provided more space for the

interactions between enzyme molecules and substrates, because PPL is quite big (the molecular weight ~50,000 D). It needs room to be bound on the surface and also needs room to bind the substrates [43]. The relative activity of the GO-Fe_3O_4@MCM-41-PPL was lower than CPS/GO-Fe_3O_4@MCM-41-PPL, but was better than GO-Fe_3O_4-PPL and PPL. It was because GO-Fe_3O_4@MCM-41 had more hydroxyl groups on the surface of magnetic mesoporous silicon for adsorption of PPL. The relative activity of the GO-Fe_3O_4-PPL ranked at the third, which was attributed to the partial reduction of GO so that less functional groups were provided to adsorb PPL. The relative activity of the non-immobilized enzyme was the lowest because the non-immobilized PPL easily suffered aggregation and denaturation.

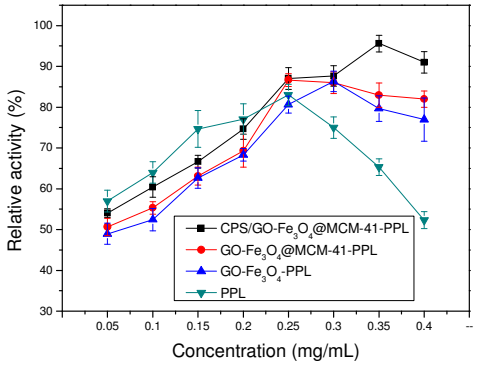

Fig. 10 Effect of the concentration on the activity of PPL and immobilized PPL

2.3.2 The effect of the pH on the relative activity of PPL

The relative activity of the non-immobilized PPL and the immobilized PPL (3.6 mg/mL) were influenced by the different pH of the PBS buffer solution, under the conditions of 30 °C for 1 h. As shown in Fig. 11, the best pH was 8.0 for CPS/GO-Fe_3O_4@MCM-41-PPL with a maximum activity 97% of initial activity. The optical pH was 7.5 for GO-Fe_3O_4@MCM-41-PPL, GO-Fe_3O_4-PPL and non-immobilized PPL. The immobilization method used for CPS/GO-Fe_3O_4@MCM-41-PPL was covalent attachment, which may reduce the conformational change of PPL, and further increase the stability for immobilized PPL in the higher pH [44]. GO-Fe_3O_4@MCM-41-PPL and GO-Fe_3O_4-PPL had better

stability compared to the non-immobilized PPL, it was believed that the microenvironment around the PPL changed after the immobilization, which was beneficial to the nucleophiles (usually Lys) in the enzyme to bind the substrates [45]. Compared to the non-immobilized PPL, the immobilized PPL had the advantages over the stability of pH, which was similar with the other reports [40-42].

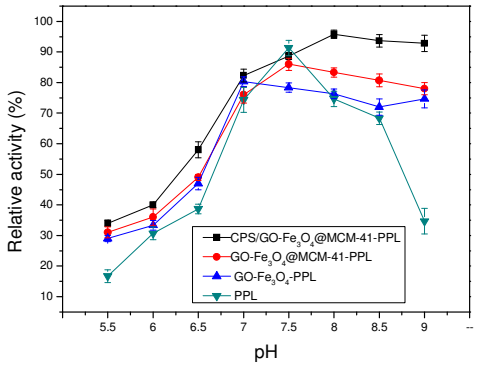

Fig. 11 Effect of pH on the activity of PPL and immobilized PPL

2.3.3 The effect of the temperature on PPL relative activity

The temperature could also affected the relative activity on the immobilized PPL and non-immobilized PPL. The results showed that the optimum temperatures were 40 °C, 35 °C, 35 °C and 35 °C, respectively for CPS/GO-Fe_3O_4@MCM-41-PPL, GO-Fe_3O_4@MCM-41-PPL, GO-Fe_3O_4-PPL and PPL. As shown in Fig. 12, CPS/GO-Fe_3O_4@MCM-41-PPL showed the best relative activity in the whole temperature range from 25 °C to 60 °C (83 % of the initial activity at 60 °C). Similarly, the covalent attachment may play an important role on the thermal stability. Secondly, the spacer arm increased the rigidity of the enzyme structure so that the most active sites were "effective fixed" [45-47]. The GO-Fe_3O_4@MCM-41-PPL exhibited the second best relative activity (72 % of the initial activity at 60 °C), the third one was GO-Fe_3O_4-PPL (69 % of the initial activity at 60 °C), which were attributed that the physical adsorption was weak so that the form of the interactions between the enzyme and support was unstable [47]. The relative activity of the non-immobilized PPL decreased rapidly (33 % of the initial activity at 60 °C) along with the increased of temperature due to the denaturation.

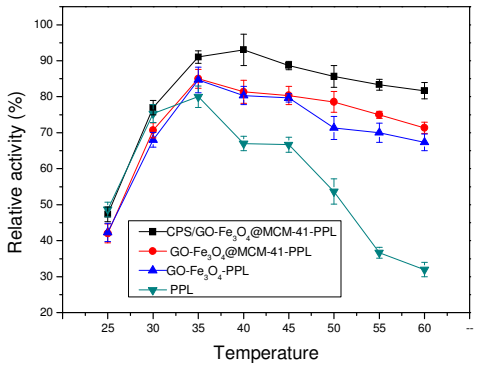

Fig. 12 Effect of temperature on the activity of PPL and immobilized PPL

2.3.4 Reusability of the immobilized PPL

The reusability for the three immobilized PPLs were analyzed and displayed in Fig. 13. The relative activity of the PPL immobilized on CPS/GO-Fe_3O_4@MCM-41 remained 87.4 % of the initial activity after ten cycles, which was better than the results from the other reports [48-49]. This could be attributed to the excellent mechanical property of graphene oxide. Also, the covalent attachment between PPL and CPS/GO-Fe_3O_4@MCM-41 could prevent desorption of PPL from the supporting material so that the relative activity remained highly [50].

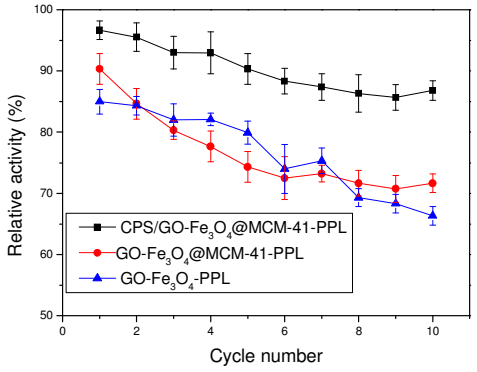

Fig. 13 Reusability of the immobilized PPL

2.3.5 Storage stability of the immobilized PPL and non-immobilized PPL

The storage stability for the non-immobilized and immobilized PPL (3.6 mg/mL) was investigated at 30 °C, pH 7.5 (0.05 M) for 56 days, and the stability test was conducted every seven days (Fig. 14). The relative activity of the CPS/GO-Fe_3O_4@MCM-41-PPL remained over 84 % of the initial activity after 56

days, which was better than the results from the other report also [51]. As speculated, non-immobilized PPL showed the poorest storage stability, and the activity was only 19 % at the same conditions. Once again, the excellent mechanical property of graphene oxide may play an important role on the stability.

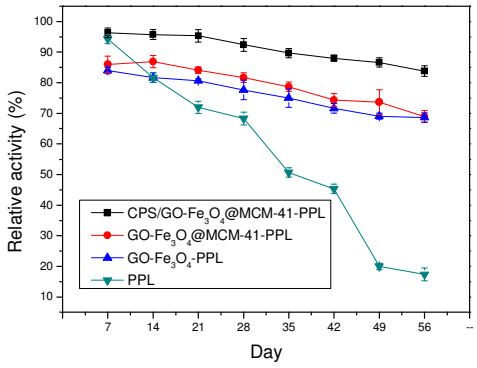

Fig. 14 Storage stability of the PPL and immobilized PPL

Conclusion

In this work, we carried out the specific immobilization strategy by use of Fe_3O_4@MCM-41, GO, CPS and PPL, which showed an excellent performance in terms of enzymology properties, such as relative activity, reusability and storage ability. The unique properties of the supporting materials such as nanoscale particle, large surface area, excellent mechanical property and good dispersion ability, provided a synergetic effect on the enzyme stabilization and activity. In addition, the steric hindrance between enzyme and supporting materials was avoided, which had positive effects on the catalyses. Based on the results obtained from this study, we propose that CPS/GO-Fe_3O_4@MCM-41 is a promising carrier for enzyme immobilization.

Acknowledgement(s). The authors are grateful for the Project supported by the National Natural Science Foundation of China (Grant No.: 51473046).

References

[1] Geim AK, Novoselov KS (2007) The rise of graphene. Nature materials 6: 183-191. doi:10.1038/nmat1849

[2] Singh V, Joung D, Zhai L, Das S, Khondaker S, Seal S (2011) Graphene based materials: past, present and future. Progress in Materials Science 56: 1178-1271. doi:10.1016/j.pmatsci.2011.03.003

[3] Bi H, Xie X, Yin K, Zhou Y, Wan S, He L, Xu F, Banhart F, Sun L, Ruoff R S (2012) Spongy graphene as a highly efficient and recyclable sorbent for oils and organic solvents. Advanced Functional Materials 22: 4421-4425. doi:10.1002/adfm.201200888

[4] Huang X, Yin Z, Wu S, Qi X, He Q, Zhang Q, Yan Q, Boey F, Zhang H (2011) Graphene-based materials: synthesis, characterization, properties, and applications. Small 7: 1876-1902. doi:10.1002/smll.201002009

[5] Xu W, Ling X, Xiao J, Dresselhaus M, Kong J, Xu H, Liu Z, Zhang J (2012) Surface enhanced Raman spectroscopy on a flat graphene surface. Proceedings of the National Academy of Sciences 109: 9281-9286. doi:10.1073/pnas.1205478109

[6] Kim IT, Magasinski A, Jacob K, Yushin G, Tannenbaum R (2013) Synthesis and electrochemical performance of reduced graphene oxide/maghemite composite anode for lithium ion batteries. Carbon 52: 56-64. doi:10.1016/j.carbon.2012.09.004

[7] Tang WW, Zeng GM, Gong JL, Liang J, Xu P, Zhang C, Huang BB (2014) Impact of humic/fulvic acid on the removal of heavy metals from aqueous solutions using nanomaterials: a review. Science of the total environment 468: 1014-1027. doi:10.1016/j.scitotenv.2013.09.044

[8] Xu P, Zeng GM, Huang DL, Feng CL, Hu S, Zhao MH, Lai C, Wei Z, Huang C, Xie GX, Liu ZF (2012) Use of iron oxide nanomaterials in wastewater treatment: a review. Science of the Total Environment 424: 1-10. doi:10.1016/j.scitotenv.2012.02.023

[9] Xu P, Zeng GM, Huang DL, Lai C, Zhao MH, Wei Z, Li NJ, Huang C, Xie GX (2012) Adsorption of Pb (II) by iron oxide nanoparticles immobilized Phanerochaete chrysosporium: equilibrium, kinetic, thermodynamic and mechanisms analysis. Chemical Engineering Journal, 203: 423-431. doi:10.1016/j.cej.2012.07.048

[10] Zhang D, Zhou C, Sun Z, Wu L, Tung C, Zhang T (2012) Magnetically recyclable nanocatalysts (MRNCs): A versatile integration of high catalytic activity and facile recovery. Nanoscale 4: 6244-6255. doi:10.1039/C2NR31929B

[11] Mazur M, Barras A, Kuncser V, Galatanu A, Zaitzev V, Turcheniuk KV, Woisel P, Lyskawa J, Laure W, Siriwardena A, Boukherroub R, Szunerits S (2013) Iron oxide magnetic nanoparticles with versatile surface functions based on dopamine anchors. Nanoscale 5: 2692-2702. doi:10.1039/C3NR33506B

[12] Gawande MB, Branco PS, Varma RS (2013) Nano-magnetite (Fe_3O_4) as a support for recyclable catalysts in the development of sustainable methodologies. Chemical Society Reviews 42: 3371-3393. doi:10.1039/C3CS35480F

[13] Garcia J, Zhang Y, Taylor H, Cespedes O, Webb ME, Zhou DJ (2011) Multilayer enzyme-coupled magnetic nanoparticles as efficient, reusable biocatalysts and biosensors. Nanoscale 3: 3721-3730. doi:10.1039/C1NR10411J

[14] Mendes AA, Oliveira PC, de Castro HF (2012) Properties and biotechnological applications of porcine pancreatic lipase. Journal of Molecular Catalysis B: Enzymatic 78: 119-134. doi:10.1016/j.molcatb.2012.03.004

[15] Moradzadegan A, Ranaei-Siadat SO, Ebrahim-Habibi A, Barshan-Tashnizi M, Jalili R, Torabi S F, Khajeh K (2010) Immobilization of acetylcholinesterase in nanofibrous PVA/BSA membranes by electrospinning. Engineering in Life Sciences 10: 57-64. doi:10.1002/elsc.200900001

[16] Gómez JL, Bastida J, Máximo MF, Montiel MC, Murcia MD, Ortega S (2011) Solvent-free polyglycerol polyricinoleate synthesis mediated by lipase from Rhizopus arrhizus. Biochemical Engineering Journal 54: 111-116. doi:10.1016/j.bej.2011.02.007

[17] Fernández-Fernández M, Sanromán MÁ, Moldes D (2013) Recent developments and applications of immobilized laccase. Biotechnology advances 31: 1808-1825. doi:10.1016/j.biotechadv.2012.02.013

[18] Zhou Z, Piepenbreier F, Marthala VRR, Karbacher K, Hartmann M (2015) Immobilization of lipase in cage-type mesoporous organosilicas via covalent bonding and crosslinking. Catalysis Today 243: 173-183. doi:10.1016/j.cattod.2014.07.047

[19] Xu J, Sun J, Wang Y, Sheng J, Wang F, Sun M (2014) Application of iron magnetic

nanoparticles in protein immobilization. Molecules 19: 11465-11486. doi:10.3390/molecules190811465

[20] Zhao F, Li H, Jiang Y, Wang X, Mu X (2014) Co-immobilization of multi-enzyme on control-reduced graphene oxide by non-covalent bonds: an artificial biocatalytic system for the one-pot production of gluconic acid from starch. Green Chemistry 16: 2558-2565. doi:10.1039/C3GC42545B

[21] Mosafa L, Moghadam M, Shahedi M (2013) Papain enzyme supported on magnetic nanoparticles: Preparation, characterization and application in the fruit juice clarification. Chinese Journal of Catalysis 34: 1897-1904. doi:10.1016/S1872-2067(12)60663-9

[22] Shao YB, Jing T, Tian JZ, Zheng YJ, Shang MH (2015) Characterization and optimization of mesoporous magnetic nanoparticles for immobilization and enhanced performance of porcine pancreatic lipase. Chemical Papers 69: 1298-1311. doi:10.1515/chempap-2015-0142

[23] Hummers Jr WS, Offeman RE (1958) Preparation of graphitic oxide. Journal of the American Chemical Society 80: 1339-1339. doi:10.1021/ja01539a017

[24] Bradford MM (1976) A rapid and sensitive method for the quantitation of microgram quantities of protein utilizing the principle of protein-dye binding. Analytical biochemistry 72: 248-254. doi:10.1016/0003-2697(76)90527-3

[25] Zhu J, Xu M, Meng X, Shang K, Fan H, Ai S (2012) Electro-enzymatic degradation of carbofuran with the graphene oxide-Fe_3O_4-hemoglobin composite in an electrochemical reactor. Process Biochemistry 47: 2480-2486. doi:10.1016/j.procbio.2012.10.006

[26] Liu Q, Shi J, Cheng M, Li G, Cao D, Jiang G (2012) Preparation of graphene-encapsulated magnetic microspheres for protein/peptide enrichment and MALDI-TOF MS analysis. Chem. Commun 48: 1874-1876. doi:10.1039/C2CC16891J

[27] Li X, Zhu H, Feng J, Zhang J, Deng X, Zhou B, Zhang H, Xue D, Li F, Mellors NJ, Li Y, Peng Y (2013) One-pot polylol synthesis of graphene decorated with size-and density-tunable Fe_3O_4 nanoparticles for porcine pancreatic lipase immobilization. Carbon 60: 488-497. doi:10.1016/j.carbon.2013.04.068

[28] Zubir NA, Yacou C, Motuzas J, Zhang XW, Costa JCDA (2014) Structural and functional investigation of graphene oxide-Fe_3O_4 nanocomposites for the heterogeneous Fenton-like reaction. Scientific reports 4. doi: 10.1038/srep04594

[29] Dementjev AP, De Graaf A, Van de Sanden MCM, Maslakov KI, Naumkin AV, Serov AA (2000) X-ray photoelectron spectroscopy reference data for identification of the C_3N_4 phase in carbon–nitrogen films. Diamond and related materials 9: 1904-1907. doi: 10.1016/S0925-9635(00)00345-9

[30] Matsuoka M, Isotani S, Mansano RD, Sucasaire W, Pinto RAC, Mittani JCR, Ogata K, Kuratani N (2012) X-Ray Photoelectron Spectroscopy and Raman Spectroscopy Studies on Thin Carbon Nitride Films Deposited by Reactive RF Magnetron Sputtering. World Journal of Nano Science and Engineering 2: 92. doi: 10.4236/wjnse.2012.22012

[31] Patra AK, Dutta A, Bhaumik A (2012) Highly Ordered Mesoporous TiO2-Fe_2O_3 Mixed Oxide Synthesized by Sol–Gel Pathway: An Efficient and Reusable Heterogeneous Catalyst for Dehalogenation Reaction. ACS applied materials & interfaces 4: 5022-5028. doi:10.1021/am301394u

[32] Bai LZ, Zhao DL, Xu Y, Zhang JM, Gao YL, Zhao LY, Tang JT (2012) Inductive heating property of graphene oxide–Fe_3O_4 nanoparticles hybrid in an AC magnetic field for localized hyperthermia. Materials letters 68: 399-401. doi: 10.1016/j.matlet.2011.11.013

[33] Peng X, Xu F, Zhang W, Wang J, Zeng C, Niu M, Chmielewska E (2014) Magnetic Fe_3O_4@ silica–xanthan gum composites for aqueous removal and recovery of Pb^{2+}. Colloids and Surfaces A: Physicochemical and Engineering Aspects 443: 27-36. doi: 10.1016/j.colsurfa.2013.10.062

[34] Dong Y, Zhang H, Rahman ZU, Su L, Chen XJ, Hu J, Chen XG (2012) Graphene oxide–Fe_3O_4 magnetic nanocomposites with peroxidase-like activity for colorimetric detection of glucose. Nanoscale 4: 3969-3976. doi:10.1039/C2NR12109C

[35] Ma H, He J, Evans DG, Duan X (2004) Immobilization of lipase in a mesoporous reactor based on MCM-41. Journal of Molecular Catalysis B: Enzymatic 30: 209-217. doi: 10.1016/j.molcatb.2004.04.007

[36] Yang J, Hu Y, Jiang L, Zou B, Jia R, Huang H (2013) Enhancing the catalytic properties of porcine pancreatic lipase by immobilization on SBA-15 modified by functionalized ionic liquid. Biochemical Engineering Journal 70: 46-54. doi:10.1016/j.bej.2012.09.016

[37] Xie G, Xi P, Liu H, Chen F, Huang L, Shi Y, Hou F, Zeng Z, Shao C, Wang J (2012) A facile chemical method to produce superparamagnetic graphene oxide–Fe_3O_4 hybrid composite and its application in the removal of dyes from aqueous solution. Journal of Materials Chemistry 22:

1033-1039. doi:10.1039/C1JM13433G

[38] Zhang W, Shi X, Zhang Y, Gu W, Li B, Xian Y (2013) Synthesis of water-soluble magnetic graphene nanocomposites for recyclable removal of heavy metal ions. Journal of Materials Chemistry A 1: 1745-1753. doi:10.1039/C2TA00294A

[39] Li Z, Xie K, Slade RCT (2001) High selective catalyst CuCl/MCM-41 for oxidative carbonylation of methanol to dimethyl carbonate. Applied Catalysis A: General 205: 85-92. doi:10.1016/S0926-860X(00)00546-9

[40] Su J, Cao M, Ren L, Hu C (2011) Fe_3O_4-graphene nanocomposites with improved lithium storage and magnetism properties. The Journal of Physical Chemistry C 115: 14469-14477. doi: 10.1021/jp201666s

[41] Zhang DH, Li YQ, Peng LJ, Chen N (2014) Lipase immobilization on magnetic microspheres via spacer arms: Effect of steric hindrance on the activity. Biotechnology and Bioprocess Engineering 19: 838-843. doi: 10.1007/s12257-013-0495-x

[42] Lin TW, Dai CS, Hung KC (2014) High Energy Density Asymmetric Supercapacitor Based on NiOOH/$Ni_3S_{2/3}$D Graphene and Fe_3O_4/Graphene Composite Electrodes. Scientific reports 4. doi:10.1038/srep07274

[43] Ozyilmaz G (2009) The effect of spacer arm on hydrolytic and synthetic activity of Candida rugosa lipase immobilized on silica gel. Journal of Molecular Catalysis B: Enzymatic 56: 231-236. doi:10.1016/j.molcatb.2008.05.008

[44] Tang T, Fan H, Ai S, Han R, Qiu Y (2011) Hemoglobin (Hb) immobilized on amino-modified magnetic nanoparticles for the catalytic removal of bisphenol A. Chemosphere 83: 255-264. doi:10.1016/j.chemosphere.2010.12.075

[45] Mateo C, Palomo JM, Fernandez-Lorente G, Guisan JM, Fernandez-Lafuente R (2007) Improvement of enzyme activity, stability and selectivity via immobilization techniques. Enzyme and Microbial Technology 40: 1451-1463. doi:10.1016/j.enzmictec.2007.01.018

[46] Chattopadhyay K, Mazumdar S (2000) Structural and conformational stability of horseradish peroxidase: effect of temperature and pH. Biochemistry 39: 263-270. doi: 10.1021/bi990729o

[47] Garcia−Galan C, Berenguer−Murcia Á, Fernandez−Lafuente R, Rodrigues RC (2011) Potential of different enzyme immobilization strategies to improve enzyme performance. Advanced Synthesis & Catalysis 353: 2885-2904. doi: 10.1002/adsc.201100534

[48] Xu Y, Zhou G, Wu C, Li T, Song H (2011) Improving adsorption and activation of the lipase immobilized in amino-functionalized ordered mesoporous SBA-15. Solid State Sciences 13: 867-874. doi:10.1016/j.solidstatesciences.2011.03.003

[49] Wang C, Zhou G, Xu Y, Chen J (2011) Porcine pancreatic lipase immobilized in amino-functionalized short rod-shaped mesoporous silica prepared using poly(ethylene glycol) and triblock copolymer as templates. The Journal of Physical Chemistry C 115: 22191-22199. doi: 10.1021/jp206836v

[50] Sharma RK, Monga Y, Puri A (2014) Magnetically separable silica@Fe_3O_4 core–shell supported nano-structured copper (II) composites as a versatile catalyst for the reduction of nitroarenes in aqueous medium at room temperature. Journal of Molecular Catalysis A: Chemical 393: 84-95. doi:10.1016/j.molcata.2014.06.009

[51] Zhang GH, Ma J, Wang J, Li Y, Zhang GL, Zhang FB, Fan XB (2014) Lipase immobilized on graphene oxide as reusable biocatalyst. Industrial & Engineering Chemistry Research 53: 19878-19883. doi: 10.1021/ie503596j